MISR radiometric uncertainty analyses and their utilization within geophysical retrievals

C.J. Bruegge, N. L. Chrien, D.J. Diner, R.A. Kahn, J. V. Martonchik

Abstract. The Multi-angle Imaging SpectroRadiometer (MISR) instrument is to be launched with the Earth Observing System EOS-AM I spacecraft in 1998. Demanding specifications include a requirement that the instrument be calibrated, and placed on an accurate radiometric scale, to within 3% (I σ) uncertainty, for incident radiances near the upper end of a camera's dynamic range. Error components, including signal-to-noise, goodness of fit to a quadratic calibration equation, and quality of the experimental conditions (i.e., range and number of radiometric levels used to provide the calibration), have all been investigated, After the component error parameters are identified, they arc flagged as contributing to onc or more of the absolute, ham-to-band relative, camera-to-camera relative, or pixel-to-pixel relative uncertainties. Preflight radiometric uncertainty results arc summarized here, and the approach for providing these for the on-orbit calibrations is discussed. Geophysical product retrievals make usc of these uncertainty values. An example of how this uncertainty analysis is incorporated into a retrieval algorithm is presented.

1. Introduction

The MISR instrument has been designed and built by the Jet Propulsion Laboratory (JPL), to be launched in 1998 as one of five instruments on the first Earth Observing System platform (EOS-AM 1). Details of the instrument design and scientific objectives arc given in [1]. The instrument consists of nine cameras, cacb with a unique view angle to Earth. Each camera makes usc of four charge-cotrplcd device (CCD) line arrays, filtered to spectral bands which arc measured to be 446, 558, 672, and 866 nm (as determined from a solar weighted, in-band moments analysis). These arc termed respectively Bands 1-4, or Blue, Green, Red and Near-lnfrarcd (NIR). '1'here exist 1504 active elements pcr line array, with 36 channels (nine cameras and 4 spectral bands) for the instrument. Samples of the contents of the CCD serial registers, termed "overclock pixels" arc taken following the active pixel read. They provide a measure of the dynamic video offset bias. The final output of the camera is provided in the form of digital numbers (DN), quantized to 14-bits of precision.

Each of the nine flight cameras was built and tested in series. Verification of boresight alignment, focus, and effective focal length was followed by radiometric anti spectral calibration, and polarization response verification. Testing was

C.J. Bruegge, N. L. Chrien, D.J. Diner, R.A. Kahn, J.V. Martonchik: Jet Propulsion Laboratory, California Institute of Technology

Metrologia
Submitted November 25, 1997

done under vacuum conditions, at temperatures predicted for the flight environment. The CCD focal planes are actively controlled to -5° C.

During radiometric calibration the relationship between an incident radiance field and camera digital output is measured. The radiometric scale is established preflight (and in-flight) for MISR using detector standards. For preflight testing two types of detector standards arc used [2]. A QED-200 (made of United Detector Technology inversion layer diodes) is used to measure sphere output for MISR spectral Elands I and 2; a QED- 150 (made of Hamamatsu p-on-n photodiodes) is used for Bands 3 and 4. (For the flight calibration, custom devices have been built, in-order to minimize the size of the photodiodes [3].) Each standard is made of three silicon photodiodes, mounted in a light-trap configuration so as to collect the light reflected at each air/ detector interface. Each photodiode is designed for 100% internal quantum efficiency for the wavelength regions at which they arc operated. These standards are used with filters of the same spectral bandpass design as the flight cameras, and with a known field-of-view, established with a precision aperture tube. Traceability to Système international (S1) units is established through the measurement protocols of current, apertures, and aperture distances. JPL maintains working standards of voltage, resistance, and length which arc traceable to the National Institute of Standards and Technology (NISI') or other international standards that arc recognized by NIST. The filter transmittance for the standards are measured by a dual-beam spectrometer, accurate to within 0.5%. The internal quantum efficiency and reflectance loss of the standards are assumed to be unity and zero respectively, with an uncertainty of 0.1% pcr the manufacturer's specification. The accuracy of these trap devices has been well established in the literature [4], [5].

In addition to these standards, a flat-field source is required for radiometric calibration. For preflight calibration, we use an integrating sphere 1.6 m (65") in diameter that has a 76x23 cm (30x9") exit port and a 30 cm (12") external sphere with a variable aperture at the entrance port to the large sphere. The sphere is sequenced through a number of lamp-on settings, allowing digital data to be collected at twelve radiometric levels, evenly spaced within the dynamic range of each spectral channel. Operationally, the sphere is initially turned on to its maximum intensity setting and allowed to warm up for 20 minutes. After data acquisition, tbc remaining output levels arc achieved quickly since all bulb transitions are from onto off. The sphere output radiance is established at each of its preprogrammed output levels using the standards. This is clone prior to each camera calibration. The standards view the sphere through the vacuum chamber window. The camera is then inserted into the thermal vacuum chamber, also viewing the sphere through the window. Sixty-four repetitions of data arc taken at each level for noise-analysis, and the procedure for the full-on to lowest output level cycle to be repeated three times to guarantee that the needed data arc acquired and as a consistency check on the calibration. A broadband photo iode, mounted so as to view the sphere back-wall, is used to verify sphere stability during a particular data acquisition run.

With these data, the coefficients in the calibration equation can be determined for each pixel of each spectral channel. For MISR this is done using a quadratic calibration equation. This functional form produces lower residuals than a linear fit, significant at the lower end of the response range. The relationship used in both calibration and Level1 radiance retrieval is:

$$G_2(\mathcal{L}^{std})^2 + G_1 \mathcal{L}^{std} + G_0 = D - DN_o \quad (1)$$

where

- $\mathcal{L}^{std}$ [W m^{-2} sr^{-2} μm^{-1}] is the incident radiance weighted by the spectral response profile. The profile used is termed the "standardized response function", and is an average of the profiles measured for a particular spectral band.
- DN is the camera digital number,
- G_2, G_1, and Go are best fit parameters to the measured radiative transfer curve, anti
- DN_o is the video offset signal, unique for each iinc of data, and measured by the overclock readout for that line.

For tbc MISR cameras, the CCD response is nearly linear and the coefficients G_0 and G_2 are small (G. typically ranges from -5 to 10 DN; G_2 is typically 0.001 DN/ (W m^{-2} sr^{-2} μm^{-1})^2). To first order the camera response is given by the G_1 coefficient, which ranges from about 20 to 40 DN/ W m^{-1} μm^{-1} sr^{-1} (see [2]).

In addition to producing radiometric coefficients, the calibration team also provides radiance products uncertainties. These include absolute radiance uncertainty, and band-to-band relative, carncra-to-camera relative, and pixel-to-pixel relative uncertainties. Both the coefficients and radiance uncertainties are compiled in a data file called the Ancillary Radiometric Product (ARP) [6]. M ISR geophysical retrieval algorithms (which produce aerosol, land-surface, and cloud products) make use of these uncertainties during standard processing **[7], [8].** Because MISR uncertainty values are used in science product generation, their computation must be well-documented and reviewed. This paper describes the error analysis that was performed for MiSR preflight radiometric calibration. In order to reduce systematic errors, MISR makes use of multiple calibration approaches. In a subsequent section, a description of how coefficients are combined from the various processing pathways is given. The final section contains an example of a science algorithm which makes use of the radiometric uncertainty values.

2. Uncertainty analysis

2.1 *Mathematical development*

We begin [his section by defining the terms absolute and relative (band-to-band, camera-to-camera, and pixel-to-pixel) uncertainties, as used by the MISR community. The term "relative uncertainty" is used to denote the uncertainty in the ratio of two observables. For clarity wc do not usc the term "relative uncertainty" to refer to the absolute uncertainty, normalized by the value itself (i.e. $\delta L/L$). Although this is commonly done in the metrology community, our approach dots not conflict with commonly referenced guidelines (see [9]), as they do not define or refer to the term "relative uncertainty". With this introduction wc provide the following MISR definitions:

absolute error, σ_{abs}. The deviation of a radiance measurement, L_{mea}, from truth, L_{true}: $\sigma_{abs}=L_{mea}-L_{true}$.

fractional absolute error, σ_{abs}/L_{true}. The deviation of a measurement from truth, normalized by the true value.

percentage absolute error, ε_{abs}. The deviat ion of a measurement from truth, normalized by the true value and expressed in percentage units: $\varepsilon_{abs}=(\sigma_{abs} \times 100)/L_{true}$. (The absolute errors reported to the M ISR ARP file are percentage errors).

confidence level. All MISR reported radiometric uncertainties arc given at the 1σ confidence level. Sixty-eight percent of the probability distribution is encompassed by the uncertainty estimate.

relative error, σ_{rel}. The deviation in the ratio of two measurements from the true ratio. To describe this mathematically wc let the ratio of measurements L_1 anti $1._2$ be denoted R_{rel}, and the ratio of the true values L_{true}, and $L_{true,2}$ be denoted R_{true}. Wc then have $\sigma_{rel}=R_{rel}-R_{true}$. Speci fic relative errors of interest to MISR arc:

- percentage band-to-band relative error, ε_{band}. The uncertainty in the ratio of radiances measured by two separate bands within a given camera, expressed in units of a percentage of the true ratio;
- percentage camera-to-camera relative error, ε_{cam}. The uncertainty in the ratio of radiances measured by two separate cameras of a common band, expressed in units of a percentage of the true ratio; and
- percentage pixel-to-pixel relative error, ε_{pix}. The uncertainty the ratio of radiances measured by two separate pixels within a given MISR channel, expressed in units of a percentage of the true ratio.

fractional relative error, σ_{rel}/R_{true}. The deviation of the ratio of two measurements from the true ratio, normalized by the true ratio.

percentage relative error, ε_{rel}. The difference of the ratio of two measurements from the true ratio, normalized by the true ratio and expressed in percentage units: $\varepsilon_{rel}=(\sigma_{rel}x100)/R_{true}$.

error components. The combined absolute or relative error is determined from a propagation of error analysis, equivalent to taking the root-sum-squares of individual error components. We express the error components in units of the final product (percentage uncertainty in the radiance or radiance ratio).

systematic errors. Those error components which result in a static offset between the measured and true value of a parameter, or a static offset in the ratio of two measured parameters, as compared to the true value of that parameter.

random errors. Those error components which result in a random offset between consecutive measured and true values. The contribution of these errors diminishes try the square-root of the number of averaged measurements. Fractional random crmr is the inverse of the signal-to-noise ratio.

Although we have taken care to make these distinctions, wc often refer loosely to absolute or relative errors when wc may be referring to their fractional or percentage equivalent. The text wiii clarify which is intended, if such a distinction is important to the discussion.

A mathematical development of the uncertainty algorithm further helps to define what is meant by absolute and relative error, as well as define how these parameters arc used to estimate the radiance ratio uncertainly for a particular set of observations. Let the radiance retrieved from a given camera be expressed as

$$L = L_{true}\prod(1+s_i) \approx L_{true}(1+\sum s_i), \quad (2)$$

where the s_i's arc multiplicative errors, dtrc to independent error components. Wc believe each of the error components identified for our calibration follow this multiplicative model. Further, as each of the component errors is small, the approximation given on the right-hand side of Eqn. 2 can be made. That is, the product of the errors is approximated by the sum of the error components. In practice tile values of s_i arc not known, but can be represented by their probability distribution, assumed to be a gaussian of zero mean, and 10 standard deviation of ε_i. We thus modify the approximation to acknowledge that oniy the probabilities in each error term arc known. Specifically, wc substitute the sum of the error terms with a roo-sum-square (RSS) computation to obtain:

$$<L>=L_{true}(1\pm\varepsilon_{abs}/100), \text{ where} \quad (3)$$

$$\varepsilon_{abs} = \sqrt{\sum\varepsilon^2_{abs,i}}, \quad (4)$$

and where ε_{abs} is referred to as the percentage absolute radiometric uncertainty in the estimated parameter, I., and $\varepsilon_{abs,i}$ arc the error components which contribute to the absolute radiometric uncertainty.

Now consider the relative camera-to-camera radiance, given by the expression $R_{cam}=L_1/L_2$, where L_1 and 1.$_2$ are the radiances measured from two channels of different cameras but of a common spectral band. For this case wc take the right-bar-d side expansion of Eqn. 2 and write

$$R_{cam} = \frac{L_1}{L_2} \approx \frac{L_{1,true}(1 + \sum s_{1,i})}{L_{2,true}(1 + \sum s_{2,i})}$$

$$\approx R_{true}(1 + \sum s_{1,i})(1 - \sum s_{2,i})$$

$$\approx R_{true}(1 + \sum (s_{1,i} - s_{2,i})) \quad (5)$$

We first note that any error term that is known to contribute equally to the uncertainty in L_1 and L_2 cancels (i.e., systematic errors where $s_{1i}=s_{2i}$ for a given error component index i). Next, using the same argument as above, wc assume the $s_{1,i}$'s and $s_{2,i}$'s arc all independent, and our estimate of R is based upon our estimate of the probabilities of ε. For this reason wc substitute the difference in Eqn. 5 with the RSS of the carncra-relative errors. Those error parameters which are camera-dependent arc flagged as camera-relative errors: denoted $\varepsilon_{cam,1,i}$ for camera 1 errors, and $\varepsilon_{cam,2,i}$ for camera 2 errors. We conclude:

$$<R_{cam}>=R_{true}(1\pm\varepsilon_{cam}/100), \text{ where} \quad (6)$$

$$\varepsilon_{cam} = \sqrt{\sum \varepsilon^2_{cam,1,i} + \sum \varepsilon^2_{cam,2,i}} \quad (7)$$

and ε_{cam} is the percentage camera-to-camera relative error. The uncertainty in the ratio of radiances is given by the RSS of the component camera-relative errors for the two cameras. This error (Eqns. 6 and 7) is less than the absolute error in radiance (Eqns. 3 and 4) only where the canlcra-relative errors arc small compared to the other error terms.

Similar expressions can be derived for the ratio of radiances from different bands, or the ratio of radiances from different pixels. In these cases, the appropriate error is written as the RSS of the error components that arc band-relative, or pixel-relative (that is, where the error component is a random error for the measurement of radiance in one band as compared to another, or one pixel as compared to another).

2.2 *Preflight calibration summary*

Tables 1a and 1b give the uncertainty in measured radiance, as determination from the laboratory standards. This is one error component o f the final combined absolute uncertainty. It is shown that the uncertainty in the internal QE of

the devices is on the order of 0.2%, as determined by a comparison of the response of several such standards. The largest error component is the uncertainty of filter transmittance, 0.5%.

Table la. Laboratory Standard Radiance Uncertainties, Blue and Red bands

QED-200 (Blue) UDT Inversion Layer Diodes		
Source Of Uncertainty	Uncertainty	Method
Internal QE >0.998 (40(-700 rrm)	±0.2%	Intercomparison of different diode types
Reflection Loss <20% Per Diode	±0.03%	JPL and Vendor tests
Linearity >99.8%	±0.25%	Vendor test and JPL analysis
SNR 1000	±0.1%	Test and analysis
Spectral Bandwidth ±0.1rrm	±0.3%	Cary measurements and analysis
Filter Transmission ~60%	±0.5%	Cary measurements and analysis
Out-of-band Transmission	±0.1%	Cary measurements and analysis
Étendue 3.55 X 10"4 cm^2 sr	fo.21 %	Tolerancing and inspection of fabricated parts and alignment
RSS 101'AI.	±0.72%	

Table lb. Laboratory Standard Radiance Uncertainties, Green and N1 R bands

QED- 150 (Red) Hamamatsu p-m-n Diodes		
Source Of Uncertainty	Uncertaint y	Method
Internal QE >0.996 (600-950 nm)	*O. 2%	Intercomparison of different diode types
Reflection Loss <30% Per Diode	±0.24%	JPL and Vendor tests
Linearity >99.996	±0.25%	Vendor test and JPL analysis
SNR 2000	±0.05 %	Test and analysis
Spectral Bandwidth ±0. 1 nm	±0.4%	Cary measurements and analysis
Filter Transmission -60%	0.5%	Cary measurements and analysis
Out-of-Band Transmission	±0.1%	Cary measurements and analysis
Étendue 3.55 x 10^{-4} cm^2 sr	0.21%	Tolerancing and inspection of fabricated parts and alignment
RSS TOTAL	±0.79%	

Table 2 provides a listing of all error components that apply to radiometric calibration. These uncertainties are reported at two incident illumination levels, ρ_{eq}= I.0 and ρ_{eq}=0.05. (The equivalent reflectance, ρ_{eq}, is defined as the incident radiance multiplied by π and divided by the band-weighted exe)-atmospheric solar irradiance [2].) The last four columns flag each of the error components as to type (absolute, $\varepsilon_{abs,i}$; camera-relative, $\varepsilon_{cam,c,i}$; band-relative, $\varepsilon_{band,c,i}$;

or pixel-relative, $\varepsilon_{pix\,i}$). 'I'he index c specifics the channel (i.e., an integer from 1 to 36); the index i represents the i^{th} error component. In the preflight calibration experiment, all radiometric error components were measured m modeled to be independent of channel. For this reason wc have not presented the error components for each channel - they arc identical. (The ARP allows for channel-(icpcndcnt errors, and thus maintains a more general crmr table. In particular, signal-k-noise ratio (SNR) will be specified on a pcr channel basis).

Table 2. Preflight radiometric error components

Parameter	% uncertainty at ρ_{eq}=1.0	% uncertainty at ρ_{eq}=0.05	Uncertainty type			
			Absolute, ε_{abs}	Camera - relative, ε_{cam}	Band-relative, ε_{band}	Pixel - relative, ε_{pix}
Diode radiance accuracy: internal QE, linearity, SNR, AΩ, filter transmittance	0.8	0.8	√			
Diode radiance accuracy: filter transmittance only	*0.5*	*0.5*			√	
Diode to camera out-of-band correction	1.0	1.*(I*	√			
Sphere non-uniformity correction	*0.2*	*0.2*	√	√		√
Sphere temporal stability	1.0	1.0	√	√		
Sphere color temperature stability	*0. I*	*o. I*			√	
Calibration equation fit	0.02	0.02	√			
Selection of radiometric levels	0.1	0. I	√			
SNR	0.1	0.5	√	√	√	√

The terms included in the "1'able 2 arc:

- diode radiance accuracy. MISR makes usc of commercial ligh-trapped, high quantum-c fficient photodiodes as its radiometric standards. These arc used to establish the integrating sphere output at the four M ISR spectral bands. The terms considered in ROW 2 was detailed in Table 1.

- filter transmittance. 'I'his is one component of the diode radiance uncertainty. It alone contributes to the band-to-band relative uncertainty.

- correction for diode-to-camera rru-rrf-band differences. Although the filters used for the cameras and laboratory photodiode standards arc of the same design, the final as-built responses are slightly different. These differences arc

characterized, and corrections are made with these measurements. The dominant error in the correction is the usage of a single representative spectral response function for each pixel.

• sphere non-uniformity knowledge. The sphere has been measured to be 3% different at the field-edges, as compared to smaller view angles. This output deviation with view angle is slowly varying, and thus only a few measurement points are needed to characterize this non-uniformity. This determination is used to adjust the incident radiances over the field-of-view of a given camera, The uncertainty listed is the scatter in non-uniformity measurements for the different camera cal i brat ions,

• sphere stability. Stabi lit y monitor readings arc recorded during calibration of both the sphere and the cameras. Sphere stability is 0.3% after the specified warm-up period. A larger instability is noted in the monitor readings in comparing sphere calibration runs (laboratory standards viewing the sphere), and the camera calibrations. Here the bulbs have been cycled cm and off many times. As no correction is made for either of these drifts, the combined uncertainty is 1%.

• sphere color temperature stability. Should there be a drift in the sphere bulb temperature, there would be a corresponding change in the sphere output radiance for one band relative to another. The magnitude of this error has not been characterized, except to assume it is much less than the overall sphere stability reported above. It is used in the band-relative uncertainty determination.

• calibration equation fit. This error has been determined by comparing the residuals between the measured DN, and those predicted from the calibration coefficients.

• selection of radiometric levels. The nonlinear term of the Fidelity Interval Analysis [10] is used to estimate the error due to the selection of test radiometric levels, as compared to the dynamic range of a camera.

• signal-to-noise ratio (SNR). The SNR reported here is the mean DN output ratioed to its standard deviation, as acquired when a series of observations are made of a flat-field source. The source is assumed stable during the time of data acquisition (a 2 sec. interval).

The root-sum-square (RSS) of the first column provides the absolute uncertainty, summarized in Table 3. Per Eqn. 7, the RSS of the relative error columns times the square-root of 2 gives the relative error, also summarized in l'able 3, assuming the two observables being ratioed have the same radiance val ue.

Table 3. Preflight cumulative radiometric uncertainties

Radiometric uncertainty	Actual		Requirement	
	% uncertainty at ρ_{eq}= 1.0	% uncertainty at ρ_{eq}=0.05	% uncertainty at ρ_{eq}= 1.0	% uncertainty at ρ_{eq}=0.05
Absolute, ε_{abs} [%]	1.6	1.7	3	6
Camera-to camera relative, ε_{cam} [%']	1.4	1.6	1	2
Band-to-band relative, ε_{band} [%]	0.7	1.0	1	2
Pixel-to-pixel relative, ε_{pix} [%]	0.3	0.7	0.5	1.

Tbc only calibration which was not done to specification is seen to be that Of the camera-relative calibration at ρ_{eq}= 1.0. The error for this case is dominated by the sphere temporal stability (change in output between the time of sphere calibration and camera test data acquisition). Clearly, a more accurate approach would have been to usc a radiance stabilized sphere, or onc monitored by temperature stabilized filtered monitoring photodiodes. We expect the in-flight measured uncertainties to bc closer to the requirement, as better methods will be available from orbit. For example, multiple cameras will view the calibration targets simultaneously. Additionally, the AirMISR camera, which flies on an ER-2 aircraft, can provide accurate camera-relative calibrations [11], and histogram equalization can provide accurate pixel-relative calibrations. The latter experiment collects images over a large number of Earth scenes. These are then binned, for each pixel, into counts versus a given DN range. For pixels in close enough proximity such that atmospheric differences, due to their view angle differences, are negligible, a relative calibration is obtained by computing the pixel-dcpcrrdcnt scaler that would allow all histograms to be superimposed.

2.3 *Pixel averaging*

The ARP contains the absolute and relative uncertainties ε_{abs}, ε_{cam}, ε_{band}, and ε_{pix} as computed by the above described algorithms. These arc given at 15 specific equivalent reflectance levels defined by the ARP, and for each camera anti band. Since the MISR instrument operates in Global Mode for much of an orbit, and as this mode transmits pixel-averaged data for many channels, the uncertainty parameters may overestimate the radiance uncertainties. This is because SNR is a random error and decreases with pixel averaging. In order to allow the science processing algorithms to utilize the best estimate of radiance uncertainties, the RSS of all error components excluding SNR, is provided. These parameters arc denoted $\varepsilon_{abs\_am\_ind}$, $\varepsilon_{cam\_am\_ind}$, $\varepsilon_{band\_am\_ind}$, and $\varepsilon_{pix\_am\_ind}$, where the suffix "am_ind" denotes “averaging-~lodc independent". They arc also given for 15 equivalent reflectance levels and 36 instrument channels. To compute these uncertainty parameters from the preflight data, the RSS of the first eight parameters from Table 2 arc RSSed (if flagged for the particular absolute or relative uncertainty parameter). From I’able 2 wc would

obtain the values 1.6, 1.0, 0.5, and 0.2 for these averaging-mode independent parameters. The science algorithms can then include the SNR radiance error component using the value appropriate for the number of pixels averaged, SNR_{am}. Here the notation SNR_{am} is used to denote that SNR is a function of the "averaging mode", or the number of pixels averaged. Thus,

$$\varepsilon_{abs} = \sqrt{\varepsilon^2_{abs\_am\_ind} + (100/SNR_{am})^2} \quad . \tag{8}$$

When the parameters $\varepsilon_{cam\ am\_ind}$ and SNR_{am}, have values that are identical **for two channels, wc find the** camera-relative **uncertainty from:**

$$\varepsilon_{cam} = \sqrt{2}\ \sqrt{\varepsilon^2_{cam\_am\_ind} + (100/\ SNR_{am}\ )2} \tag{9}$$

To see how pixel averaging affects the radiometric uncertainties, reference is made to Figure 1, which shows how photon, quantization and other electronic noise vary as a function of the number of pixels averaged. In the model [2], quantization noise is not reduced with averaging mode, as arc the other components. For this reason there is little change in the total noise as one averages more than 4x4 pixels. 'l'able 4 makes usc of SNR_{am} as computed from this model. The uncertainties do not vary more than O. 1% in going from the 4x4 to 16x16 pixel averaging case, for equivalent reflectance inputs greater than 0.005 (i.e., 0.5%). For this reason, it is sufficient to extract SNR_{am} from the 1x1, 1x4, 2x2, or 4x4 cases given in the ARP.

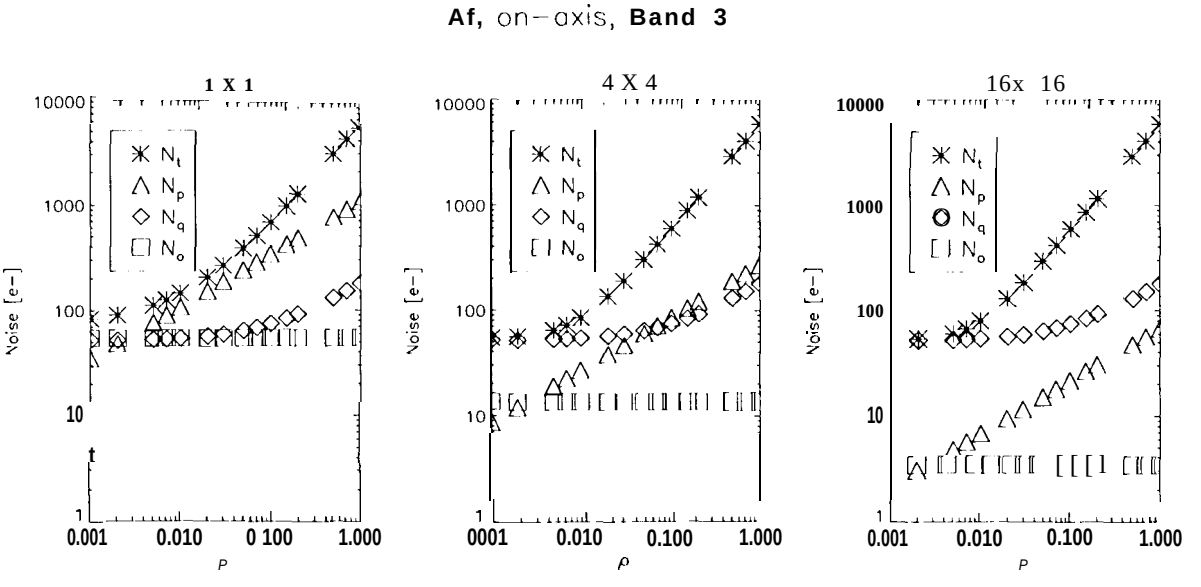

Figure 1. Photon, quantization, and other noise as a function of I x 1, 4x4, and 16x16 pixel averaging.

Table 4. Camera-relative error reduction d_{LIC} to pixel averaging

equivalent reflectance, ρ_{eq}	SNR_{am} crmr component [%] versus averaging mode			combined percentage camera relative error [%] versus averaging mode		
	1x1	4x4	16x16	1X1	4x4	16x16
0.001	7.5	4,9	4.7	10.6	7.1	6.8
0.002	4.0	2.5	2.4	5.9	3.8	3.6
0.005	I .9	1.0	1.0	3.1	2. I	*2.0*
0.007	1.5	0.8	0.7	*2.6*	1.8	1.8
0.01	1.2	0.6	0.5	*2.2*	1.6	1.6
0.02	0.8	0.3	0.3	1.8	1.5	*I .5*
0.03	0.6	0.2	0.2	1.7	1.5	*1.5*
0.05	*0.5*	0.2	0.1	1.6	1.s	1.5
0.07	*0.4*	(). 1	(). 1	*I .6*	*1.5*	*1.4*
0.1	*0.3*	0.1	0.1	*1.5*	*I .4*	*I .4*
0.15	*0.3*	0.1	0.1	*1.5*	*1.4*	*I .4*
0.2	*0.2*	0. I	0.0	*I .s*	*1.4*	*I .4*
0.5	*0.1*	0.0	0.0	*1.5*	*1.4*	1.4
0.7	*0. I*	*0.0*	*0.0*	1.5	*1.4*	1.4
1.	*0.1*	*0.0*	*0.0*	1.4	1.4	1.4

3. In-flight calibration

3.1 *Combining multiple methodologies*

For the in-flight program, a complete error analysis will be done on cacb calibration methodology. These include calibrations using data acquired from the On-Board Calibrator (OBC), rcflcctancc-based vicarious calibrations, AirMISR underflights, and histogram equalization. Our plans call for making use of all data, weighted by their uncertainties.

The error budgets for these multiple methodologies is given in "1'able 5. The error components for OBC include diode radiance accuracy ***(2%*** radiance uncertainty, including degradation during mission life), diffuse panel spatial non-

uniformity (0.2%), panel relative bi-directional reflectance factor (BRF) (2%), panel flatness (0.01 96), calibration equation fit (0.02%), radiometric levels (0.01 %), and SNR.

Table 5. In-flight radiometric error budgets

Methodology	% uncertainty at ρ_{eq}=1.0			
	Absolute	Camera-to-camera	Band-to-band	Pixel-to-pixel
OBC	2.8	2.8	*0.8*	*0.4*
Reflectance-based vicarious	5.0 (D camera); 3.0 (nadir)			
AirMISR		1.0		
Histogram equalization				*0.5*
Requirement	3	1	1	*0.5*

Not all methods can provide a determination of both absolute and relative values of the gain coefficients. As the reflcc(ancc-based vicarious technique measures surface reflectance and atmospheric transmittance over one ground instantaneous-field-of-view (GIFOV) element, it determines the gain for one MISR pixel for each of 36 channels. Using a relative response model of the array, this determination is used to derive an estimate of the array-averaged response. We combine this with the measure of the average gain as determined from OBC data using the equations:

$$\bar{G}_l \sum_{=}(\bar{G}_{l\ \ i}/\sigma_i^2) \Big/ \sum(1/\sigma_i^2) \tag{lo}$$

$$\sigma^2 = \frac{1}{N}\sum\sigma_i^2 \tag{11}$$

where i is the summation index over methodologies (in this case 2), $\bar{G}_{l,i}$ is the channel average gain coefficient, and $\bar{G}_l$ is the combined channel average gain coefficient. Let us assume we have six OBC observations and one vicarious observations which believe to be accurate to the budgets given in Table 5. For a D camera, wc believe our final calibration will be uncertain to 3.2%; for the A camera to 2.8%. (D refers to a lens design that is used for the two most oblique-vicwirlg cameras; A refers to a lens design that is used for the nadir and two near-nadir viewing cameras.) A simple average of the uncertainties is taken, as these errors arc dominated by the systematic errors, and do not reduce with the number of observations.

4. Aerosol retrieval over dark water

Onc way in which the MISR team is planning to take advantage of the care given to calibration is by incorporating instrument uncertainties directly into the retrieval of geophysical quantities. We use the statistical formalism of chi-

squared tests. In our aerosol retrievals, for example, we compare the measured radiances with model radiances, calculated for a range of possible aerosol amounts, compositions, and size distributions. In the chi-squared tests, if the difference between the measured radiances and a comparison model are comparable to the instrument uncertainty, agreement between the mode] and the observation is judged to bc significant. Absolute, camera-to-camera, and band-to-band instrument uncertainties are automatically read from the radiometric calibration files into the MISR retrieval algorithm, anti arc used in calculating the chi-squared test variables. Examples of this can be found in land-sur face, cloud, and aerosol retrieval algorithms. Onc specific example is described bet-c.

The M ISR approach to retrieving aerosol over dark water is described in [7] and [12]. The algorithm compares top-of-atmosphere (TOA) measured reflectances with those computed from a model atmosphere. Each model atmosphere, in turn, is computed by varying the aerosol optical depth, effective article radius, and the real and imaginary indices of refraction. Four specific tests arc used to dccidc whether a comparison model is consistent with the measurements. Each test is based upon the χ^2 statistical formalism [13].

The first criterion to be used to find the best-fit[ing optical depth is minimization of the reduced χ^2_{abs} parameter, calculated as a function of optical depth as follows:

$$\chi^2_{abs}(\tau) = \frac{\sum_{\lambda=3}^{4}\left[\sum_{j=1}^{9} w_j \cdot \frac{[\rho_{MISR}(\lambda, j) - \rho_{model}(\lambda, j)]^2}{\sigma^2_{abs}(l, j)}\right]}{\sum_{\lambda=3}^{4}\left[\sum_{j=1}^{9} w_j\right]} \qquad (12)$$

where ρ_{MISR} are MISR equivalent reflectances, computed by taking the median over the subregions in the 17.6 km x 17.6 km region which passed through all screens, ρ_{model} are the model TOA equivalent reflectances for the aerosol mixture, and σ_{abs} is the absolute radiometric uncertainty in ρ_{MISR}. The sum over j corresponds to the cameras and the sum over λ corresponds to wavelength, and for- dark water includes only bands 3 and 4, the wavelengths at which the dark water surface is assumed tn have negligible reflectance. Eqn. 12 also contains weighting factors w_j. For the dark waler retrievals, the w_j's are the inverse of the cosine of the view angle of camera j, providing a greater weighting of the more oblique cameras to take advantage of the longer atmospheric slant path

The value of σ_{abs} is obtained by using calibration uncertainty information provided in the MISR Ancillary Radiometric Product. To calculate σ_{abs} corresponding to equivalent reflectance ρ_{MISR}, wc first linearly interpolate the tabulated values of $\varepsilon_{abs\ am\ ind}$ and SNR_{4x4} to this equivalent reflectance. Denoting these interpolated values $\varepsilon_{abs\_am\_ind}(\rho_{MISR})$ and $SNR_{4x4}(\rho_{MISR})$, we then have

$$\sigma^2_{abs} = \rho^2_{MISR}\left\{\left(\frac{\varepsilon_{abs\_am\_ind}(\rho_{MISR})}{100}\right)^2 + \frac{1}{SNR_{4x4}(\rho_{MISR})}\right\}^2 \quad (13)$$

Once χ^2_{abs} has been minimized, its absolute value **establishes** whether the candidate aerosol model provides a good fit to the measurements. In theory, a value of $\chi^2 \leq 1$ indicates a good fit. However, to allow for unmodeled sources of uncertainty a value of $\chi^2 \leq 2$ is defined as an acceptable fit.

The second test makes use of the angular shape normalized to a reference camera (*refcam*), which emphasizes camera-to-camera geometric differences:

$$\chi^2_{geom}(\tau) = \frac{\sum_{\lambda=3}^{4}\left[\sum_{j=1}^{8} w_j \frac{\left(\frac{\rho_{MISR}(\lambda, j)}{\rho_{MISR}(\lambda, refcam)} - \frac{\rho_{model}(\lambda, j)}{\rho_{model}(\lambda, refcam)}\right)^2}{\sigma^2_{geom}(\lambda, j)}\right]}{\sum_{\lambda=3}^{4}\left[\sum_{j=1}^{8} w_j\right]} \quad (14)$$

where σ_{geom} (a dimensionless quantity) is the uncertainty in the measured camera-to-camera equivalent reflectance ratio, given by:

$$\sigma^2_{geom}(\lambda, j) = \frac{\sigma^2_{cam}(\lambda, j)}{\rho^2_{MISR}(\lambda, refcam)} + \frac{\rho^2_{MISR}(\lambda, j)}{\rho^2_{MISR}(\lambda, refcam)} \frac{\sigma^2_{cam}(\lambda, refcam)}{\rho^2_{MISR}(\lambda, refcam)} \quad (15)$$

in which σ_{cam} is the relative camera-to-camera calibration uncertainty in the equivalent reflectance ρ_{MISR}. Eqn. 15 is derived by propagating the instrument errors [13]. The summation j over cameras excludes camera *refcam*. This reference camera is preferentially An (the nadir). For dark water, the summation over λ in Eqn. 14 includes only bands 3 and 4.

The value of σ_{cam} is obtained by using calibration uncertainty information provided in the MISR Ancillary Radiometric Product. To calculate σ_{cam} corresponding to equivalent reflectance ρ_{MISR}, we again linearly interpolate. This is now done to obtain the values $\varepsilon_{cam\_am\_ind}$ and SNR_{4x4} at this equivalent reflectance, Denoting these interpolated values $\varepsilon_{cam\_am\_ind}(\rho_{MISR})$ and $SNR_{4x4}(\rho_{MISR})$, we then have

$$\sigma^2_{cam} = \rho^2_{MISR}\left\{\left(\frac{\varepsilon_{cam\_am\_ind}(\rho_{MISR})}{100}\right)^2 + \frac{1}{(SNR_{4x4}(\rho_{MISR}))}\right\}^2 \quad (16)$$

1'wo other goodness-of-fit parameters are the angular shape 01 the spectral ratio relative to Band 3, χ^2_{spec}, anti a maximum deviation parameter, χ^2_{maxdev}, or the channel at which the observed equivalent reflectance is most different from the model equivalent reflectance.

Successful aerosol models arc those for which all four metrics, χ^2_{abs}, χ^2_{geom}, χ^2_{spec}, and χ^2_{maxdev} arc $\leq$ the threshold value of 2. This threshold val ue may be adjusted pending further theoretical sensitivity studies and experience with actual MISR data.

Acknowledgments. The work described in this paper is being carried out by the Jet Propulsion 1.aboratory, California Institute of Technology, under contract with the National Aeronautics anti Space Administration.

References

i. D. Diner, J. Beckert, T. Reilly, 'I'. Ackerman, C. Bruegge, J. Conel, R. Davies, S. Gerstl, H. Gordon, R. Kahn, J. Martonchik, J.-P. Muller, R. Myneni, B. Pinty, P. Sellers, and M. Verstraete, "Muiti-angle Imaging SpectroRadiometer instrument description and experiment overview," submitted IEEE Trans. Geosci. Remote Sensing, special EOS issue, 1998.

2. Carol J. Bruegge, Valerie G. Duval, Nadine L. Chrien, Robert P. Korechoff, Barbara J. GaitIcy, and Eric B. Hochberg, "MISR prelaunch instrument calibration and characterization results, " submitted IEEE Trans. Geosci. Remote Sensing, special EOS issue, 1998.

3. C.J. Bruegge, V.G. Duval, N. I.. Chrien, and D.J. Diner, "Calibration Plans for the Multi-angle Imaging SpectroRadiometer (M ISR)," Metrologia, 30(4), 2 i 3-22 i, 1993.

4. N.P. Fox and J.E. Martin, Appl. Opt., Vol 29(3 1), 4686-4692, 1990.

5. J. Geist, E.F. Zalewski, anti A.R. Schaefer, Appl. Opt. 19, 3795, 1980.

6. R.M. Woodhouse, C.J. Bruegge, B.J. Gaitley, G. Saghri, and N. Chrien, "Multi-angle Imaging SpectroRadiometer (MISR) Ancillary Radiometric Product (ARP)," Earth Observing System II, Proc. SPIE **3117**, San Diego, CA, July 1997.

7. J.V. Martonchik, D.J. Diner, R. Kahn, M. Verstraete, B. Pinty, H. Gordon, and T. Ackerman, "Techniques for the retrieval of aerosol properties over land and ocean using multi-angle imaging, " submitted IEEE Trans. Geosci. Remote Sensing, special EOS issue, 1998.

8. J. Martonchik, D. Diner, B. Pinty, M. Verstraete, H. Gordon, R. Myneni, anti Y. Knyazikhin. "Determination of land anti ocean reflective and radiative properties using multi-angle measurements, " submitted IEEE Trans. Geosci. Remote Sensing, special EOS issue, 1998.

9. B.N. Taylor and C. Ii. Kuyatt, Guidelines for Evaluating the Uncertainty 01 NIST Measurement Results, NIST Technical Note 1297, 1994.

10. Chrien, N. C.I,., C.J. Bruegge, and B.R. Barkstrom (1993). Estimation of calibration uncertainties for the Multi-angle Imaging SpectroRadiometer (M ISR) via fidelity intervals. In *Sensor Systems for the Early Earth Observing System Platforms*, Proc. SPIE 1939, April, 114-125.

11. D.J. Diner, L.M. Barge, C.J. Bruegge, T.G. Chrien, J. E. Conel, M. L. Eastwood, J.D. Garcia, M.A. Hernandez, C.G. Kurzweil, W.C. Ledeboer, N.D. Pignatano, C.M. Sarture, and B.G. Smith, "The Airborne Multi-angle SpectroRadiometer (AirMISR): instrument description and first results, " submitted IEEE Trans. Geosci. Remote Sensing, special EOS issue, 1998.

12. D.J. Diner, W.A. Abdou, T.P. Ackerman, K. Crean, H.R. Gordon, R.A. Kahn, J.V. Martonchik, S.R. McMuldroch, S.R. Paradise, B. Pinty, M.M. Verstraete, M. Wang, and R.A. West, Level 2 Aerosol Retrieval Algorithm Theoretical Basis, Jet Propulsion Laboratory Internal Document JPL D-11 400, Rev. C.

13. Bevington, Philip R. and D. Keith Robinson (1996). Data Reduction and Error Analysis for the Physical Sciences, Second Edition. McGraw Hill, Inc.